Journal of Colloid and Interface Science 329 (2009) 182–187

Contents lists available at ScienceDirect

Journal of Colloid and Interface Science

www.elsevier.com/locate/jcis

Effect of chemical structure of interface modifier of TiO_2 on photovoltaic properties of poly(3-hexylthiophene)/TiO_2 layered solar cells

Chih-Wei Hsu [a], Leeyih Wang [a,b,*], Wei-Fang Su [a,c,*]

[a] Institute of Polymer Science and Engineering, National Taiwan University, Taipei, 10617, Taiwan
[b] Center for Condensed Matter Sciences, National Taiwan University, Taipei, 10617, Taiwan
[c] Department of Materials Science and Engineering, National Taiwan University, Taipei, 10617, Taiwan

ARTICLE INFO

Article history:
Received 23 June 2008
Accepted 2 October 2008
Available online 9 October 2008

Keywords:
Interface modification
Hybrid solar cells
Self-assembled monolayer
TiO_2
Poly(3-hexylthiophene)

ABSTRACT

Two classes of phosphonic acid-bearing organic molecules, 2-oligothiophene phosphonic acid and ω-(2-thienyl)alkyl phosphonic acid were adopted as interface modifiers (IMs) of the TiO_2 surface, to increase its compatibility with poly(3-hexylthiophene) (P3HT). The self-assembled monolayers of these molecules on titania surface were characterized by making contact angle measurements and X-ray photoelectron spectroscopy (XPS). Atomic force microscopic (AFM) images revealed that the adsorption of IMs effectively smoothes the TiO_2 surface. Both photoluminescence (PL) spectroscopy and PL lifetime measurements were made to investigate the photoinduced properties of the TiO_2/IM/P3HT layered-junction. The PL quenching efficiency increased with the number of thiophene rings and as the alkyl chain-length in IMs decreased. Meanwhile, the decline in the PL lifetime followed a similar trend as the PL quenching efficiency. Additionally, the power conversion efficiency (PCE) of the ITO/TiO_2/IM/P3HT/Au devices was examined by measuring their photocurrent density–applied voltage (J–V) curves. The experimental results indicated that the short-circuit current density (J_{SC}) increased with the number of thiophene units and as the hydrocarbon chain-length in IMs decreased. However, the open-circuit voltage (V_{OC}) of the devices slightly fell as the energy level of the highest occupied molecular orbital (HOMO) of IM decreased. The PCE of the device with 2-terthiophene phosphonic acid was 2.5 times that of the device with 10-(2-thienyl)decyl phosphonic acid.

1. Introduction

Traditional fuel energy resources are limited and generate harmful waste products in the atmosphere. Hence, alternative eco-friendly energy sources are receiving increasing attention. Of all substitute energy sources, solar power is most attractive because of its abundance and the consistency of sunlight. In 1950s, Chapin et al. at Bell laboratories developed the first crystalline silicon solar cell with a solar-energy conversion efficiency of 6% [1]. However, the relatively high cost of manufacturing these silicon cells has prevented them from extensive use. Moreover, another disadvantage of silicon cells is the use of toxic chemicals during manufacturing. Accordingly, the development of low-cost organic solar cells is urgent.

Conjugated polymer-based solar cells represent a growing area of research that holds promise for the creation of low-cost flexible devices for commercial application. In particular, polymer solar cells offer numerous advantages in the area of fabrication, such as low cost, roll-to-roll production of large-area flexible solar cell. Given these advantages, the development of polymer solar cells is expected to have a major impact [2–6]. Polymer solar cells are usually fabricated from a photoactive layer which comprises an interpenetrating network of donor and acceptor materials [7,8]. This bulk-heterojunction structure has been widely studied and developed, because it can greatly increase the donor/acceptor interfacial area, promoting the dissociation of photogenerated excitons into charge carriers and enabling holes and electrons to be transported and collected. One of the most effective to date is the polymer/[6,6]-phenyl-C-61-butyric acid methyl ester (PCBM) blend system that has demonstrated a certified power conversion efficiency of around 5% [9]. Another promising approach is to use inorganic semiconductors as acceptors. In organic/inorganic bulk heterojunction photovoltaic cells, the active layer is constructed by blending conjugated polymer as donor with inorganic semiconductors as acceptor. This approach is gaining popularity because of its advantages: firstly, the hybrid material combines the advantages of high electron mobility, stability of inorganic materials and the solution-processing of polymers; secondly, the compensated light harvest of nanocrystals and conjugated polymers enlarges the ab-

* Corresponding authors at: Center for Condensed Matter Sciences, National Taiwan University, Taipei, 10617, Taiwan. Fax: +886 2 23696221.
E-mail addresses: leewang@ntu.edu.tw (L. Wang), suwf@ntu.edu.tw (W.-F. Su).

0021-9797/$ – see front matter
doi:10.1016/j.jcis.2008.10.008

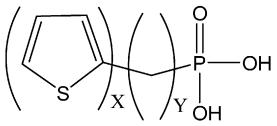

T1: X=1, Y=0
T2: X=2, Y=0
T3: X=3, Y=0
N6: X=1, Y=6
N10: X=1, Y=10

Fig. 1. The molecular structure of surface modifiers employed in this study.

sorption range, leading to the efficient conversion of sunlight [10]. In recent years, various solution-processed organic/inorganic bulk heterojunction photovoltaic cells have been reported. The inorganic particles used in those systems include CdSe [10–17], HgTe [18], TiO_2 [19–21] and ZnO [22–26] in nanosphere, nanorod or tetrapod shapes. However, when such a processing procedure has been employed, controlling the detailed morphology and dispersion of nanocrystals within the polymer has been difficult because of the incompatibility of organic polymer and inorganic semiconductor. Hence, the need for a surfactant that can control the dispersion of inorganic semiconductor nanocrystals in a wide variety of solvents and polymers is substantial [27]. In the case of CdSe and poly(2-methoxy-5-(2′-ethyl-hexyl-oxy)-*p*-phenylenevinylene) (MEH-PPV), a 1.1 nm-thick monolayer of the common surfactant, trioctylphosphine oxide (TOPO) is located on the surface of the CdSe nanocrystals, which disperse effectively in organic solvent, but sufficed to reduce electron transfer efficiency by a factor of ten [10]. W.J.E. Beek et al. used *n*-propylamine as surfactant to prepare a poly[2-methoxy-5-(3,7-dimethyloctyloxy)-1,4-phenylenevinylene] (MDMO-PPV)/ZnO bulk heterojunction. They showed that even though adding *n*-propylamine improved the film-forming properties of the blend, this addition still did not improve the performance of the photovoltaic cell [28]. Obviously, the choice of stabilizer or interface modifiers of nanocrystals is a key to improving the performance of a bulk heterojunction photovoltaic cell.

This work adopted two series of organic molecules with different chemical structures, 2-oligothiophene phosphonic acid with various thiophene rings (T-series) and ω-(2-thienyl)alkyl phosphonic acid with various alkyl chain lengths (N-series), as shown in Fig. 1, as interface modifier (IM), to investigate the structural effect of modifiers on the performance of organic/inorganic photovoltaic devices. A bilayer TiO_2/P3HT cell configuration was chosen for this study because the planar heterojunction between TiO_2 and P3HT not only eliminates complex issues concerning bulk heterojunctions such as pore filling, phase segregation and charge collection, but also ensures the optical interference profiles of devices are similar if the layers are of the same thicknesses [29,30]. Furthermore, results of studying a planar system may be directly applicable to bulk heterojunction systems.

2. Materials and methods

2.1. Synthesis of poly(3-hexylthiophene) and phosphonic acid-containing molecules as interface modifier

Phosphonic acid-containing molecules and regioregular poly(3-hexylthiophene) (P3HT) were synthesized via Grignard reaction method. The detailed synthesis and characterization procedures are provided in the Supplementary material.

2.2. Preparation of compact TiO_2 film

The ITO glass substrate (10 Ω/square) was cleaned with detergent followed by ultrasound cleaning for 15 min with deionized water, acetone and isopropyl alcohol and then drying in a vacuum oven at room temperature. A precursor solution of titanium isopropoxide-acetylacetone complexes was prepared by mixing titanium isopropoxide (0.284 g) with acetylacetone (0.2 g) in ethanol (30 ml). Precursor was deposited by the spry-pyrolysis method using N_2 as carrying gas at a flow rate of 7 L/min on a cleaned ITO glass surface preheated to 450 °C. After deposition, films were calcined under air for 5 min at 450 °C, which yielded flat TiO_2 films with a thickness of about 30 nm.

2.3. Preparation of self-assembled monolayers (SAMs) of phosphonic acid-containing molecules on compact TiO_2 film

SAMs were prepared by immersing TiO_2-coated ITO glass in an anhydrous tetrahydrofuran (THF) solution of 1 mM phosphonic acid-containing molecules for two days under ambient conditions. Substrates with SAMs were then rinsed with THF to remove residual reagents and then dried in a vacuum oven at room temperature.

2.4. Fabrication of photovoltaic devices

A chloroform solution of P3HT was spin-coated on the SAMs/TiO_2/ITO substrates. The thickness of the polymer layer was controlled by varying the spin speed and the concentration of the polymer solution. Au was then evaporated under vacuum (lower than 5×10^{-6} Torr) in an EDWARDS AUTO 306 vacuum evaporation system at 0.1 Å/s. The thickness of the gold was approximately 100 nm. The active area of each device was 4 mm × 3 mm. Finally, the devices were annealed at 140 °C for 10 min in a glove box.

2.5. Characterization

The surface wetability of SAMs/TiO_2 substrates was studied by measuring the static contact angles with a First Ten Angstroms (FTA 125) contact angle analyzer at room temperature and ambient humidity, using water as the probe liquid. A 2 μL water droplet was placed on the substrate *via* a syringe. The angle was obtained by estimating the tangent to the drop where it intersects the surface, and an average over five measurements was taken for reported contact angles. The X-ray photoelectron spectroscopic (XPS) analyses were conducted using a VG Scientific ESCALAB 250 system. Spectra were acquired at a base pressure of 10^{-9} Torr using a monochromatic Al$K\alpha$ X-ray source at 200 W. Samples were grounded to prevent charging, and charge compensation was applied. The survey scans were performed at an energy range of 0–1100 eV with a pass energy of 80 eV while core-level single spectra were collected using a pass energy of 20 eV and an acquisition time of 180 s. The binding energy was referenced to the C1s photoelectron peak of 284.6 eV.

Photoelectron spectroscopy in air (PESA) analyses were conducted using a Riken Keiki AC-2 UV photoelectron spectrometer. The UV source was 100 nW deuterium D_2 lamp with a spot diameter of 2 × 2 mm. The samples were analyzed at 22 °C, 40% relative humidity and 1012 kPa pressure.

Atomic force microscopy (AFM) was performed in air using a Digital Instruments Nanoscope IIIa Multimode atomic force microscope in tapping mode. The nominal force constant of the silicon nitride cantilever (Nanoprobes Ltd.) was 0.12 Nm^{-1}. Cyclic voltammetry was carried out using a CHI 660 Electrochemical Analyzer with carbon, a Pt plate, and Ag/Ag^+ electrode as the working,

Table 1
Optical and electrochemical properties of surface modifiers.

	T1	T2	T3	N6	N10
λ_{onset} (nm)	262	352	416	257	255
E_g (eV)	4.73	3.53	2.98	4.82	4.86
E_{ox} (V)	1.73	1.50	1.10	1.67	1.67
LUMO (eV)	−1.44	−2.41	−2.56	−1.29	−1.26
$HOMO_{CV}$ (eV)	−6.17	−5.94	−5.54	−6.11	−6.11
$HOMO_{AC-2}$ (eV)	−6.05	−5.93	−5.72	−6.03	−6.03

counter and reference electrodes, respectively, in a 0.1 M tetrabutylammonium perchlorate (TBAP) acetonitrile solution. Ultraviolet–visible (UV–vis) absorption spectra were measured on a HITACHI U-3410 spectrophotometer. Photoluminescence (PL) spectra were obtained and life-time measurements were made using a JOBIN YVON Fluorolog Tau-3 lifetime system. All current density–voltage (J–V) characteristics of the devices were measured using a Keithley 2400 source measurement unit. The light source was a 300 W xenon lamp (Oriel). Under AM1.5G conditions, the radiant light power was adjusted with respect to a standard reference cell (monocrystalline silicon solar cell with KG-5 filter, calibrated at NREL, Colorado, USA) to one-sun intensity (100 mW/cm^2).

3. Results and discussion

3.1. Energy levels of interface modifiers.

The optical bandgaps (E_g) of interface modifiers were estimated from the onset absorption wavelengths (λ_{onset}) in their UV–vis spectra using Eq. (1):

$$E_g = 1240/\lambda_{onset}\ (\text{eV}). \quad (1)$$

Table 1 presents these absorption onset wavelengths and energy gap results of IMs. As the number of thiophene rings increased, the onset absorption wavelength of T-series modifiers increased markedly from 270 nm to 416 nm, corresponding to a decrease of energy gap from 4.6 to 3.53 eV due to the increase in conjugation length. As expected, the N-series molecules exhibited a wider energy gap than T-series molecules but the increase in alkyl length from 6-carbon to 10-carbon only slightly raised the bandgap from 4.87 nm to 4.91 eV. Cyclic voltammetry measurements were made to determine the oxidation potentials of IMs and the HOMO and LUMO values of IMs were estimated using Eqs. (2) and (3) [31]:

$$\text{HOMO} = -\big((E_{ox}) - \text{ferrocene}(E_{ox,1/2})\big) - 4.8\ \text{eV}, \quad (2)$$

$$\text{LUMO} = \text{HOMO} + E_g\ (\text{eV}). \quad (3)$$

The oxidation potentials and HOMO and LUMO values of IMs are summarized in Table 1. It reveals that the oxidation potentials fell from 1.73 to 1.10 V for T-series molecules as the number of thiophene rings increased, leading to a decrease in LUMO and an increase in HOMO energy levels. This observation clearly indicates the extension of the conjugated backbone in oligothiophene had enormous effect on its energy gap as well as HOMO and LUMO levels. In addition, a photoelectron spectrometer (Riken Keiki AC-2) was employed to determine the ionization potential of the interface modifiers in solid state. Fig. S-3 plots the square root of the counting rate (CR) as a function of the photon energy, and the photoemission threshold energy was determined from the crossing point of the background and the yield line. The HOMOs of T1, T2, T3, N6 and N10 were found out to be 6.05, 5.93, 5.72, 6.03 and 6.03 eV, respectively. The trend in HOMO values of surface modifiers measured by cyclic voltammetry were consistent with those measured by PESA.

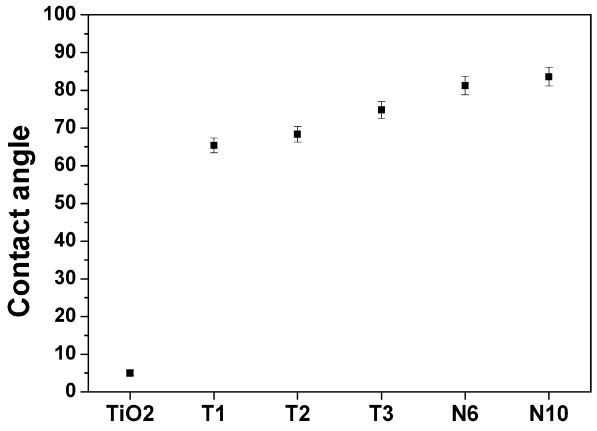

Fig. 2. Static contact angle of water on the surface modifier-covered TiO_2 substrates.

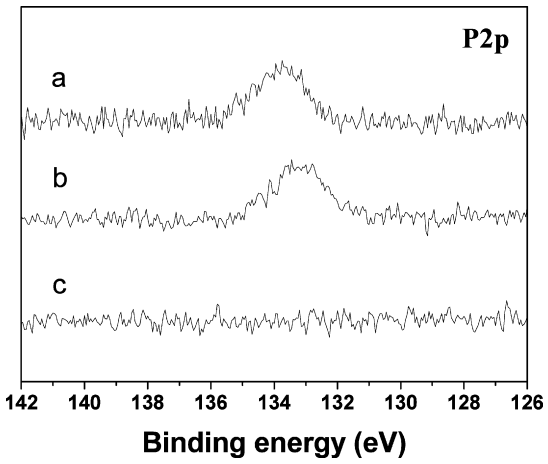

Fig. 3. XPS spectra of (a) bulk T3 (free acid), (b) T3-covered TiO_2 substrate and (c) bare TiO_2 substrate.

3.2. Characterization of SAMs on compact TiO_2 film

Fig. 2 depicts the static contact angles of water on IM-covered TiO_2 substrate. The results show that the static water contact angle increased abruptly from about 5° for bare TiO_2-coated ITO glass to 65° for IM-modified TiO_2-coated ITO glass, suggesting that the formation of a thin layer of IMs on top of TiO_2 altered the surface from hydrophilic to hydrophobic. Furthermore, the contact angle data indicated that a longer alkyl chain (N10) and more thiophene rings (T3) of IMs corresponded to greater hydrophobicity of the corresponding self-assembled monolayers (SAMs).

Fig. 3 displays high-resolution XPS spectra of P2p for SM molecules, IM-covered TiO_2 substrate and bare TiO_2 substrate. No observable P2p signal in the range of 126–142 eV from bare TiO_2 substrate was found in Fig. 3c. In Fig. 3a, a binding energy signal at 133.7 eV from bulk IM molecules was attributed to the P2p of phosphonic acid group. When bare TiO_2 substrate absorbed IM molecules, the P2p signal was shifted from 133.7 eV to 133.2 eV (Fig. 3b), suggesting a change in the chemical structure of the phosphate headgroup upon coordination with the surface. M. Textor et al. reported similar results in the octadecyl phosphoric acid/tantalum oxide system, which were key indicators of the presence of a phosphonate monolayer on the TiO_2 surface [32].

AFM was employed to examine the surface roughness of both bare TiO_2 and IM-modified TiO_2 substrates. The scan range of all AFM images was 1 × 1 μm and the Z range was 5 nm. The TiO_2 substrate that was prepared by the spray-pyrolysis method was very smooth with a root-mean-square (RMS) roughness of around

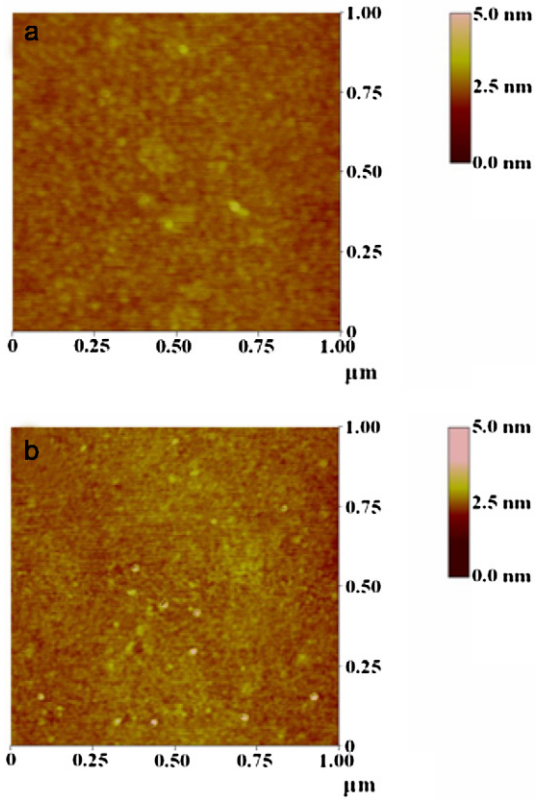

Fig. 4. AFM images of (a) bare TiO_2 and (b) T3-modified TiO_2 substrates.

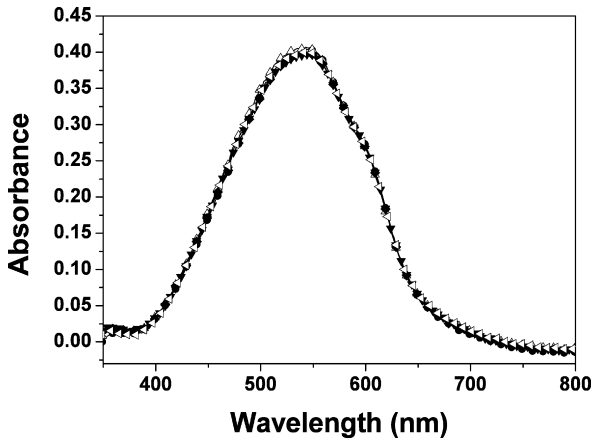

Fig. 5. UV–vis spectra of P3HT/surface modifier-covered TiO_2 bilayer junction: (○) T1, (△) T2, (▼) T3, (◆) N6, (□) N10.

0.19 nm (Fig. 4a). When the TiO_2 substrate was modified with IMs, the RMS roughness of the thus formed IM-covered TiO_2 substrate was slightly lower. Fig. 4b shows a typical of compact monolayer of T3 that was formed on the TiO_2 substrate with an RMS roughness of about 0.14 nm. This result demonstrates that IMs can smooth the TiO_2 substrate.

3.3. Characterization of P3HT/SM/TiO_2 layered junctions

Fig. 5 shows the solid-state UV–vis spectra of the P3HT/IM-modified TiO_2 bilayer junctions. It exhibits a broad absorption spectrum of P3HT from 400 to 700 nm. All of samples in which the TiO_2 adsorbed different IM molecules showed similar spectra with a maximum absorption wavelength at 540 nm, indicating that the interface modifier does not contribute significantly to light harvesting.

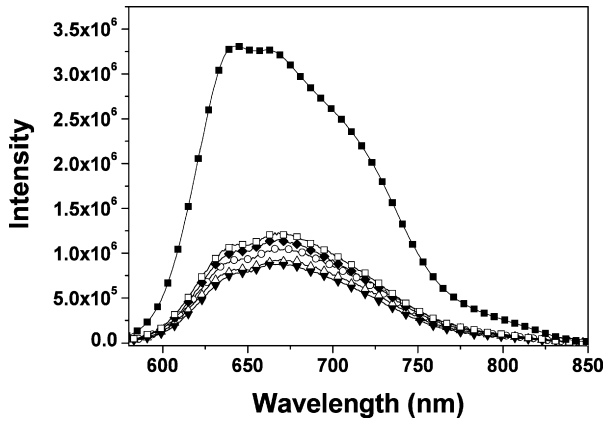

Fig. 6. Photoluminescence spectra of (■) pristine P3HT and P3HT/surface modifier-covered TiO_2: (○) T1, (△) T2, (▼) T3, (◆) N6, (□) N10.

Table 2
Approximate photoluminescence quenching efficiencies and PL lifetime measurements of P3HT/surface modifier-covered TiO_2 bilayer junctions.

	Pure P3HT	T1	T2	T3	N6	N10
Quenching efficiency (%)	–	70	73.8	75.6	68	65.3
Lifetime, τ (ns)	1.18	1.05	1.02	0.98	1.08	1.1

Photoluminescence quenching in P3HT/IM-modified TiO_2 bilayer junctions is a useful indication of the degree of success of exciton dissociation [33,34]. The photoluminescence (PL) intensities of pure P3HT and P3HT films spin-coated onto IM-modified TiO_2 substrates were compared. As expected, Fig. 6, the PL intensity of the P3HT/SM/TiO_2 layered junctions was much lower than that of pristine P3HT, suggesting PL quenching caused by charge separation. The PL intensity decreased as the alkyl chain length of SMs (T1, N6, N10) decreased and the number of thiophene rings of IMs increased (T1, T2, T3).

The PL quenching efficiencies of each film were determined by comparing the PL integrated area under each curve. The approximate quenching efficiencies (η_q) are defined as follows.

$$\eta_q = 1 - (A_{PL,SM}/A_{PL,P3HT}), \quad (4)$$

where, $A_{PL,SM}$ and $A_{PL,P3HT}$ denote the area under the PL curves of P3HT/IM-covered TiO_2/ITO and pristine P3HT/ITO, respectively. The calculated results are summarized in Table 2. For each of the samples in Table 2, the quenching efficiency decreased from 70 to 65.3% as the alkyl chain length of the N-series IMs increased but increased from 70 to 75.6% as the number of thiophene rings of T-series IMs increased, indicating that higher efficiency of charge separation at the P3HT/TiO_2 interface can be achieved by choosing interface modifiers with either shorter insulating main-chain or longer conjugated backbone. Photoinduced electron transfer can also be inferred from lifetime measurement. Table 2 presents the PL lifetime measurements. It reveals that the PL lifetime (τ) declined as the number of thiophene rings in the T-series IMs increased and increased as the alkyl chain length of the N-series IMs increased. The trend in both PL and lifetime data is probably because the decrease in the LUMO of the IMs eases the charge transfer between P3HT and TiO_2 upon illumination. Also, reducing the non-conducting alkyl chain length of IMs reduces the insulating barrier distance between the donor and the acceptor and promotes photo-induced charge transfer efficiency.

3.4. Photovoltaic measurements

Fig. 7 plots IPCE measurements of devices with various IMs. The figure shows that the IPCE curve of the device with the

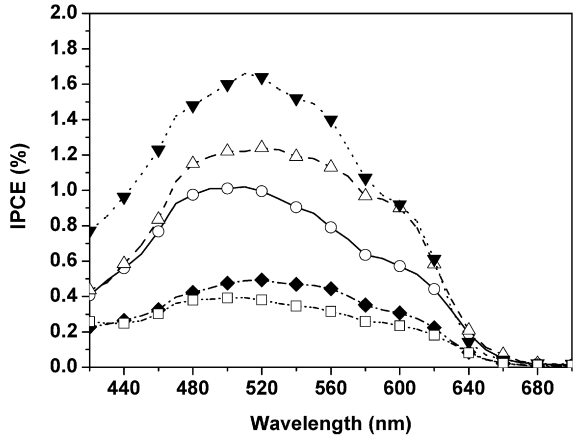

Fig. 7. IPCE spectra of layered devices ITO/TiO_2/surface modifier/P3HT/Au: (○) T1, (△) T2, (▼) T3, (◆) N6, (□) N10.

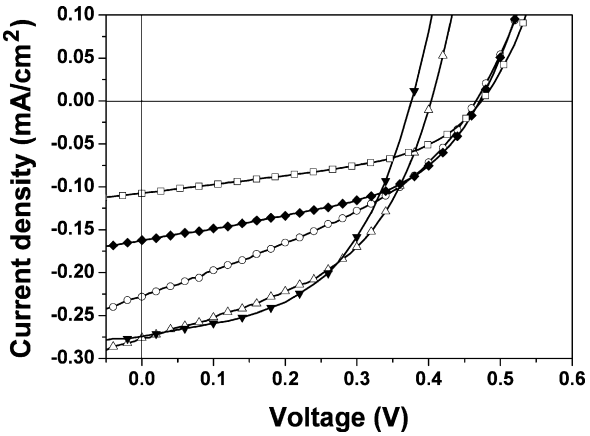

Fig. 8. J–V curves of layered devices ITO/TiO_2/surface modifier/P3HT/Au: (○) T1, (△) T2, (▼) T3, (◆) N6, (□) N10.

Table 3
Photovoltaic properties of layered devices ITO/TiO_2/surface modifier/P3HT/Au.

	T1	T2	T3	N6	N10
V_{OC} (V)	0.46	0.4	0.38	0.47	0.48
J_{SC} (mA/cm^2)	0.228	0.276	0.274	0.162	0.108
FF (%)	36.8	46.7	50.6	46.7	45.7
η (%)	0.038	0.054	0.060	0.036	0.024

P3HT/IM/TiO_2-layered junction with T-series molecules had higher IPCE than the device with the N-series molecules. In particular, the P3HT/SM/TiO_2 layered junction device had a maximum IPCE of 1.7% at 510 nm; this maximum significantly exceeded that (0.4%) of the P3HT/N10-TiO_2 device, implying that N6 and N10 molecules, which with long alkyl chains, create an insulating barrier and reduce the charge separation and transport efficiencies.

Fig. 8 plots the J–V curves of the P3HT/IM-modified TiO_2 bilayer junctions. Table 3 summarizes the effect of changing the species of SMs on the photovoltaic characteristics. It shows that increasing the number of thiophene rings in the T-series SMs seemed to decrease V_{OC} but increased J_{SC}. Additionally, V_{OC} increased slightly with the alkyl chain length of IMs but J_{SC} decreased. These V_{OC} results are consistent with the variation in the LUMO of IMs, suggesting the presence of IM molecules can somehow influence the energy level of an acceptor. The short-circuit current density was attributed to the fact that increasing the number of thiophene rings lowered the LUMO of IMs to around the LUMO of P3HT, promoting charge transfer from P3HT to TiO_2, and to the fact that reducing the alkyl chain length of IMs lowered the insulating barrier between donor and acceptor, also promoting charge transfer between P3HT and TiO_2.

4. Summary

The influence of the chemical structure of phosphonic acid-containing interface modifiers of TiO_2 on the photoinduced properties of the layered-junction TiO_2/IM/P3HT was investigated. Both PL and PL lifetime measurements suggested that the photoinduced transfer of electrons from P3HT to TiO_2 increased as the conjugation length of molecular backbone increased or as the non-conjugated chain-length in SMs decreased. Moreover, the molecular structure of IMs strongly affected the cell performance of the layered device ITO/TiO_2/IM/P3HT/Au through their energy levels and charge transfer ability. The J_{SC} increased as the number of thiophene rings increased and the length of the insulating chain in IMs decreased. Although the drop in the LUMO level of IMs enhanced the photocurrent, it was also accompanied by a reduction in V_{OC}. Accordingly, the increment in J_{SC} and the decline in V_{OC} must be traded off to optimize cell performance. These experimental findings provide a reference and design strategy that support a promising means of stabilizing inorganic particles in the fabrication of high-efficiency organic/inorganic photovoltaic devices.

Acknowledgments

The authors would like to thank National Taiwan University and the National Science Council of Republic of China for financially supporting this research.

Supplementary material

The online version of this article contains additional supplementary material.

Please visit DOI: 10.1016/j.jcis.2008.10.008.

References

[1] D.M. Chapin, C.S. Fuller, G.L. Pearson, J. Appl. Phys. 74 (1954) 230.
[2] A. Fujii, A. Zakhidov, V. Borovkov, Y. Ohmori, K. Yoshino, Jpn. J. Appl. Phys. 35 (1996) L1438.
[3] K. Tada, M. Onoda, H. Nakayama, K. Yoshino, Synth. Met. 102 (1999) 982.
[4] W. Feng, T. Umeda, A. Fujii, X. Wang, K. Yoshino, Jpn. J. Appl. Phys. 43 (2004) 3473.
[5] W.Y. Wong, Macromol. Chem. Phys. 209 (2008) 14.
[6] W.Y. Wong, X.Z. Wang, Z. He, A.B. Djurišić, C.T. Yip, K.Y. Cheung, H. Wang, C.S.K. Mak, W.K. Chan, Nat. Mater. 6 (2007) 521.
[7] J.J.M. Halls, C.A. Walsh, N.C. Greenham, Nature 376 (1995) 498.
[8] G. Yu, J. Gao, C.J. Hummelen, F. Wudl, A.J. Heeger, Science 270 (1995) 1789.
[9] G. Li, V. Shrotriya, J. Huang, Y. Yao, T. Moriarty, K. Emery, Y. Yang, Nat. Mater. 4 (2005) 864.
[10] N.C. Greenham, X.G. Peng, A.P. Alivisatos, Phys. Rev. B 54 (1996) 17628.
[11] W.U. Huynh, X.G. Peng, A.P. Alivisatos, Adv. Mater. 11 (1999) 923.
[12] W.U. Huynh, J.J. Dittmer, A.P. Alivisatos, Science 295 (2002) 2425.
[13] W.U. Huynh, J.J. Dittmer, W.C. Libby, G.L. Whiting, A.P. Alivisatos, Adv. Funct. Mater. 13 (2003) 73.
[14] J. Liu, T. Tanaka, A.P. Alivisatos, K. Sivula, J.M.J. Frechet, J. Am. Chem. Soc. 126 (2004) 6550.
[15] C.M. Yang, C.M. Wu, H.H. Liao, Appl. Phys. Lett. 90 (2007) 133509.
[16] Y.G. Li, W. Meng, L.D. Zhang, Appl. Phys. Lett. 76 (2000) 2011.
[17] S. Link, Z.L. Wang, M.A. El-Sayed, J. Phys. Chem. B 104 (2000) 7867.
[18] S. Gunes, H. Neugebauer, N.S. Sariciftci, J. Roither, M. Kovalenko, Adv. Funct. Mater. 16 (2006) 1095.
[19] C.Y. Kwong, A.B. Djurisic, P.C. Chui, K.W. Cheng, W.K. Chan, Chem. Phys. Lett. 384 (2004) 372.
[20] L.H. Slooff, M.M. Wienk, J.M. Kroon, Thin Solid Films 451 (2004) 634.
[21] W. Feng, Y. Feng, Z. Wu, Jpn. J. Appl. Phys. 44 (2005) 7494.
[22] W.J.E. Beek, M.M. Wienk, R.A.J. Janssen, Adv. Mater. 16 (2004) 1009.
[23] W.J.E. Beek, L.H. Slooff, M.M. Wienk, J.M. Kroon, R.A.J. Janssen, Adv. Funct. Mater. 15 (2005) 1703.
[24] W.J.E. Beek, M.M. Wienk, R.A.J. Janssen, J. Mater. Chem. 15 (2005) 2985.

[25] W.J.E. Beek, M.M. Wienk, R.A.J. Janssen, Adv. Funct. Mater. 16 (2006) 1112.
[26] P.A.C. Quist, L.H. Slooff, H.A. Donker, Superlattices Microstruct. 38 (2005) 308.
[27] D.J. Milliron, A.P. Alivisatos, C. Pitois, C. Edder, J.M.J. Frechet, Adv. Mater. 15 (2003) 58.
[28] W.J.E. Beek, M.M. Wienk, M. Kemerink, X. Yang, R.A.J. Janssen, J. Phys. Chem. B 109 (2005) 9505.
[29] L.A.A. Pettersson, L.S. Roman, O. Inganas, J. Appl. Phys. 86 (1999) 487.
[30] F. Nuesch, M. Carrara, L. Zuppiroli, Langmuir 19 (2003) 4871.
[31] J.H. Hou, Z. Tan, Y.J. He, C.H. Yang, Y. Li, Macromolecules 39 (2006) 4657.
[32] M. Textor, L. Ruiz, R. Hofer, A. Rossi, K. Feldman, G. Hähner, N.D. Spencer, Langmuir 16 (2000) 3257.
[33] K.M. Coakley, Y. Liu, M.D. McGehee, K.L. Frindell, G.D. Stucky, Adv. Funct. Mater. 13 (2003) 301.
[34] N.C. Greenham, X. Peng, A.P. Alivisatos, Phys. Rev. B 54 (1996) 17628.